Disrupting the blood–brain barrier by focused ultrasound induces sterile inflammation

Zsofia I. Kovacs[a,1], Saejeong Kim[a], Neekita Jikaria[a], Farhan Qureshi[a], Blerta Milo[a], Bobbi K. Lewis[a], Michele Bresler[a], Scott R. Burks[a], and Joseph A. Frank[a,b,1]

[a]Frank Laboratory, Radiology and Imaging Sciences, Clinical Center, National Institutes of Health, Bethesda, MD 20892; and [b]National Institute of Biomedical Imaging and Bioengineering, National Institutes of Health, Bethesda, MD 20892

Edited by Kevin J. Tracey, Feinstein Institute for Medical Research, Manhasset, NY, and accepted by Editorial Board Member Carl F. Nathan, November 23, 2016 (received for review September 5, 2016)

MRI-guided pulsed focused ultrasound (pFUS) combined with systemic infusion of ultrasound contrast agent microbubbles (MB) causes localized blood–brain barrier (BBB) disruption that is currently being advocated for increasing drug or gene delivery in neurological diseases. The mechanical acoustic cavitation effects of opening the BBB by low-intensity pFUS+MB, as evidenced by contrast-enhanced MRI, resulted in an immediate damage-associated molecular pattern (DAMP) response including elevations in heat-shock protein 70, IL-1, IL-18, and TNFα indicative of a sterile inflammatory response (SIR) in the parenchyma. Concurrent with DAMP presentation, significant elevations in proinflammatory, antiinflammatory, and trophic factors along with neurotrophic and neurogenesis factors were detected; these elevations lasted 24 h. Transcriptomic analysis of sonicated brain supported the proteomic findings and indicated that the SIR was facilitated through the induction of the NFκB pathway. Histological evaluation demonstrated increased albumin in the parenchyma that cleared by 24 h along with TUNEL$^+$ neurons, activated astrocytes, microglia, and increased cell adhesion molecules in the vasculature. Infusion of fluorescent beads 3 d before pFUS+MB revealed the infiltration of CD68$^+$ macrophages at 6 d postsonication, as is consistent with an innate immune response. pFUS+MB is being considered as part of a noninvasive adjuvant treatment for malignancy or neurodegenerative diseases. These results demonstrate that pFUS+MB induces an SIR compatible with ischemia or mild traumatic brain injury. Further investigation will be required before this approach can be widely implemented in clinical trials.

pulsed focused ultrasound | microbubbles | blood-brain barrier | sterile inflammation | magnetic resonance imaging

The temporal proteomic profile in response to blood–brain barrier disruption (BBBD) consists of molecular features that are common across noninfectious insults such as ischemia, trauma, or autoimmune diseases (1–7). The main purpose of the blood–brain barrier (BBB) is to maintain homeostasis, preventing the passive crossing of cells and molecules that could induce inflammation or damage to cells. The BBB consists of specialized endothelial cells connected through various tight junction proteins (TJP), astrocyte endplates, and a basement membrane. These components form part of the neurovascular unit (NVU) that is comprised of vessels, pericytes, microglia, astrocytes, and neurons along with the extracellular matrix (1, 3, 4, 8). BBBD secondary to ischemia or trauma leads to increases in endothelial caveolae and down-regulation of TJP, transcytosis of plasma proteins (i.e., albumin), and vasogenic edema (1, 6, 8–11). The presence of albumin in the parenchyma following BBBD can activate astrocytes and microglia and induce the production of cytokines, chemokines, and trophic factors (CCTFs) and cell adhesion molecules (CAMs) as observed with a sterile inflammatory response (SIR) to injury (12–15). The release of CCTFs and intercellular adhesion molecule (ICAM) following an insult can result from the transient release of damage-associated molecular patterns (DAMPs) that alter the local metabolic and physiologic processes that occur between the vasculature and the rest of the NVU (8, 13–19).

Various methods have been developed for transient BBBD to enhance the delivery of chemotherapeutic agents, antibodies, genes, and nanoparticles to the parenchyma (20–27). Invasive and noninvasive approaches have been used for drug and gene delivery into the parenchyma with or without altering BBB homeostasis. The BBB can be bypassed by direct injection or convection-enhanced delivery of drugs or viruses, but these means require surgical intervention, and the infiltration of agents into the parenchyma may be limited by diffusion (24–26). The injection of hypertonic mannitol, i.v. or via the intracarotid artery, has been used presumably to cause osmotic shrinkage and alter calcium flux in endothelial cells, resulting in disruption of the TJP and opening the BBB for drug delivery (24–26). The activation of bradykinin B2 receptors by intraarterial infusion of bradykinin or its analog RMP-7 also can result in calcium-medicated opening of the BBB and can enhance the delivery of agents (24). Paracellular and transcellular crossing of the brain–endothelium barrier also can be accomplished with directed infusion of vasogenic agents, trophic factors such as VEGF, or proinflammatory cytokines into the brain vasculature, causing alteration in BBB function (27). MRI-guided pulsed focused ultrasound (pFUS) combined with the infusion of contrast agent microbubbles (pFUS+MB) is a noninvasive technique that can cause transient BBBD in targeted brain regions and facilitate the delivery of large molecules into the parenchyma. Contrast-enhanced MR-guided pFUS+MB transiently opens the BBB in the targeted parenchyma without evidence of microhemorrhages (21, 28). It has been postulated that the BBBD following pFUS+MB results from a combination of acoustic radiation forces [i.e., soft tissue displacement exerted by ultrasound (US)]

Significance

Pulsed focused ultrasound (pFUS) with systemic microbubble (MB) infusion is a noninvasive technique that opens the blood–brain barrier (BBB) and is currently advocated for increasing drug or gene delivery in neurological diseases. The opening of the BBB by pFUS+MB resulted in immediate damage-associated molecular patterns that led to a sterile inflammation response within the parenchyma that lasted 24 h. Currently, pFUS+MB exposure is under consideration as an adjuvant in the treatment in malignancy or neurodegenerative disease. These results demonstrate that pFUS+MB induces a sterile inflammatory response compatible with ischemia or mild traumatic brain injury. Further investigation will be required before translation to clinical trials.

Author contributions: Z.I.K., S.K., and J.A.F. designed research; Z.I.K., S.K., N.J., F.Q., B.M., B.K.L., and M.B. performed research; Z.I.K., S.K., N.J., F.Q., B.M., B.K.L., M.B., S.R.B., and J.A.F. analyzed data; and Z.I.K., S.K., S.R.B., and J.A.F. wrote the paper.

The authors declare no conflict of interest.

This article is a PNAS Direct Submission. K.J.T. is a Guest Editor invited by the Editorial Board.

[1]To whom correspondence may be addressed. Email: jf5z@nih.gov or zsofia.kovacs@nih.gov.

This article contains supporting information online at www.pnas.org/lookup/suppl/doi:10.1073/pnas.1614777114/-/DCSupplemental.

and acoustic cavitation forces inducing stable MB oscillations that can be accompanied by shear stress and microstreaming (i.e., radiating forces originating from MB) or inertial cavitation with unstable oscillations and violent rapid collapse of MB at the endothelial surface resulting in decreased tight junction integrity (29, 30). pFUS+MB has been reported to cause hemodynamic alterations in the brain associated with temporary vasoconstriction, as seen with BBBD (31, 32). The molecular effects on the NVU associated with BBBD following pFUS+MB have received limited attention.

Here, we report the temporal proteomic and transcriptomic changes in the brain associated with BBBD following pFUS+MB that were consistent with an SIR within the parenchyma (14, 18, 33). Increased numbers of $TUNEL^+$ cells scattered through the targeted parenchyma, microglial and astrocyte activation, and increased ICAM up-regulation were observed within 1 h postsonication. Systemic prelabeling of macrophages with fluorescent beads before pFUS+MB allowed the detection of these cells within the sonicated parenchyma 6 d after treatment. These results indicate that BBBD by pFUS+MB induces a transient SIR as observed with trauma or damage to NVU.

Results

The major findings of this study were as follows: (*i*) pFUS+MB infusion resulted in acute BBBD observed by MRI and on histology; (*ii*) pFUS+MB rapidly (within 5 min) induced protein expression of heat-shock protein 70 (HSP70) along with the proinflammatory cytokines TNFα, IL1α, IL1β, IL18, and IFNγ, lasting 12–24 h; (*iii*) molecular analyses of pFUS+MB–treated brains revealed increased CCTFs and transcriptomic changes associated with the NFκB pathway and sterile inflammation; (*iv*) histologic analyses of pFUS+MB–treated brain showed increased numbers of $TUNEL^+$ cells, up-regulation of ICAM, and activated astrocytes and microglia up to/for 24 h postsonication injury; and (*v*) tropism of systemic $CD68^+$ macrophages to targeted brain was found several days postsonication. For this study, the pFUS+MB parameters were chosen to cause BBBD and cerebral vasculature vasospasm without causing parenchymal damage or microhemorrhages (31, 34). We demonstrate that pFUS+MB initiated a cascade of molecular profile and cellular changes consistent with the induction of a sterile inflammation in the targeted brain.

Assessment of BBBD. All animals underwent MRI before sonication to ensure that rats had normal brain ventricular anatomy (35). Following pFUS+MB, gadolinium (Gd)-enhanced T1-weighted (T1w) images demonstrated contrast enhancement in the frontal lobe demarcating the area that was harvested for molecular and histological analysis at different time points (Fig. 1*A*). Immunofluorescence (IF) staining, coinciding with areas of BBBD on MRI, revealed the increased presence of albumin at 6 h postsonication that returned to the levels in the contralateral cortex by 24 h (Fig. 1*B*). H&E staining demonstrated no evidence of microhemorrhages within the pFUS+MB–treated cortex (Fig. 1*A*).

Molecular Response to pFUS+MB. Homogenates from sonicated brains were obtained at various time points, and proteomic and transcriptomic analyses were performed. We observed no difference in mRNA levels in the sham-treated controls and contralateral brain samples from pFUS+MB–treated rats (Table S1). Molecular patterns consistent with injury or damage in the targeted brain were observed with significant elevations (measured in picograms per milliliter) in proteins, including HSP70 ($P < 0.05$, ANOVA) and IL1α, and a fivefold increase in mRNA of *Il1a* within 5–30 min following pFUS+MB exposure (Figs. 2 and 3 and see Tables S2 and S3 for a complete list of fold-changes and description for mRNA evaluated). Moreover, significant increases in the expression of IL18 protein ($P < 0.05$, ANOVA) and mRNA for *Il1b* (>21-fold) were detected between 5 and 30 min post pFUS+MB. Within 5 min after sonication, significant increases in the expression of TNFα protein along with the production of other proinflammatory factors (IFNγ, IL-2, IL-5, IL-6, IL-12p70, and IL-17) and chemotactic factors [RANTES, granulocyte colony stimulating factor (G-CSF), granulocyte macrophage colony-stimulating factor (GM-CSF), monocyte colony-stimulating factor (M-CSF), and macrophage inflammatory protein 3 alpha (MIP3α)] were detected. Within 30 min following sonication, a greater than fivefold increase was observed in mRNA for *Il1a*, *Il1b*, and *Tnf* along with immune cell trophic factors (*Ccl12*, *Cxcl1*, and *Cxcl3*), selectins (*Selp*) and CAM (*Icam1*), the Ig superfamily of receptors (*Cd83*), the high-affinity receptor (*Csf2rb*) for binding IL3, IL5, and colony-stimulating factor (CSF), and prostaglandin-endoperoxide synthase 2 (prostaglandin G/H synthase and cyclooxygenase, *Ptgs2*)

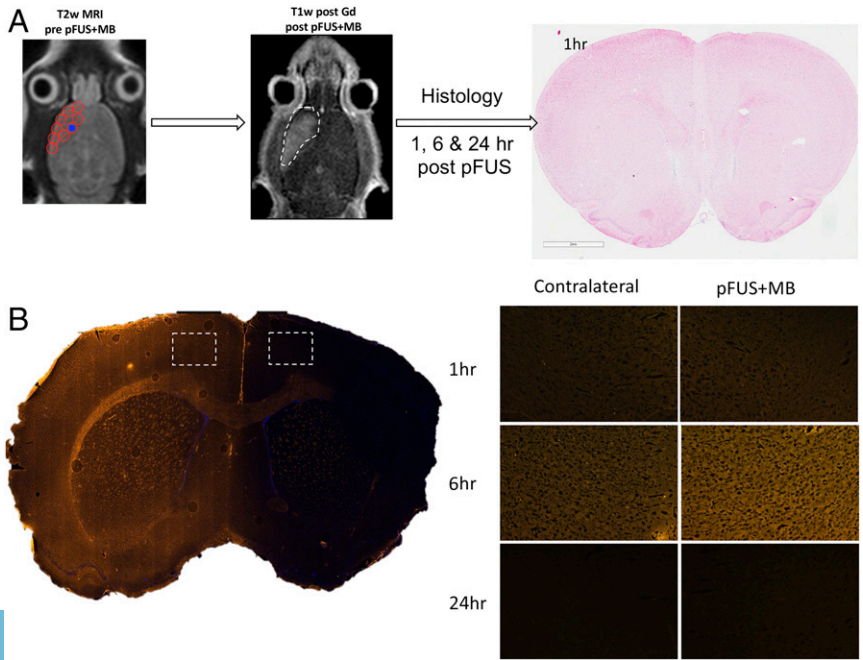

Fig. 1. BBBD by pFUS+MB. (*A*) Diagram of the experimental design for pFUS-treated rat brain for histological analysis. T2w MRI was used to target FUS with points (red circles) ~2 mm in diameter placed in the left frontal cortex anterior to the lateral ventricle. Following pFUS+MB, Gd-enhanced T1w images were obtained. The dashed white line outlines the contrast enhancement. Animals were killed 1, 6, or 24 h after sonication, and brains were collected for histology. No microhemorrhages or macroscopic alterations to morphology were observed on H&E staining. (*B*) Albumin extravasated through the open BBB with peak parenchymal accumulation occurring at 6 h post pFUS+MB.

(Fig. 3 *B* and *C*); these increases are consistent with activation of the NFκb pathway and sterile inflammation. Concurrent with the early expression of inflammatory CCTFs, significant increases ($P < 0.05$, ANOVA) in the expression of the proteins VEGF, erythropoietin (EPO), basic fibroblast growth factor (bFGF), IL4, IL10, and IL13 were also detected in the sonicated parenchyma (Fig. 2 *B* and *C*). The increased expression in VEGF would be observed with changes in vascular permeability to albumin and plasma proteins resulting from BBBD. Between 0.5 and 12 h, persistent and significant expression of cell stress-reactive proteins, pro- and antiinflammatory CCTFs, was detected in the pFUS-treated brain (Fig. 2). The increase in ICAM1 started at 2 h postsonication and persisted to 24 h ($P < 0.05$, ANOVA). Other factors, such as stromal cell-derived factor 1 alpha (SDF1α) and keratinocyte-derived chemokine (KC), were significantly elevated at a single time point from 2 to 6 h postsonication. Two hours postsonication, the protein expression of proinflammatory factors (IL2, IL6, Il12p70, IL17, and IL18) and antiinflammatory factors (IL4, and IL13, FGF) was not significantly elevated (Fig. 2). The increased mRNA expression of chemokine (C-C motif) ligand 12 (*Ccl12*) (>4- to 114-fold) and matrix metalloproteinase 9 (*Mmp9*) (greater than three- to fivefold) was mirrored by increased expression of CCTF proteins between 0.5 and 24 h postsonication. The elevation of monocyte chemotactic protein 1 (MCP-1) protein (i.e., starting at 2 h postsonication) also could have contributed to the BBB opening as well as inducing the tropism of systemic macrophages or microglia to the sonicated parenchyma (36). The expression of brain-derived neurotrophic factor (BDNF) protein was significantly ($P < 0.05$, ANOVA) increased starting at 12 through 24 h postsonication (Fig. 2*B*). Between 6 and 12 h postsonication, mRNA for Stat3 was elevated by more than twofold, presumably in response to various cytokines and growth factors (Fig. 3 *B* and *C*).

Real-time RT-PCR showed that activation of the NFκB pathway peaked at 6 h after pFUS+MB with 32 of the 39 identified mRNAs elevated significantly (by more than twofold)

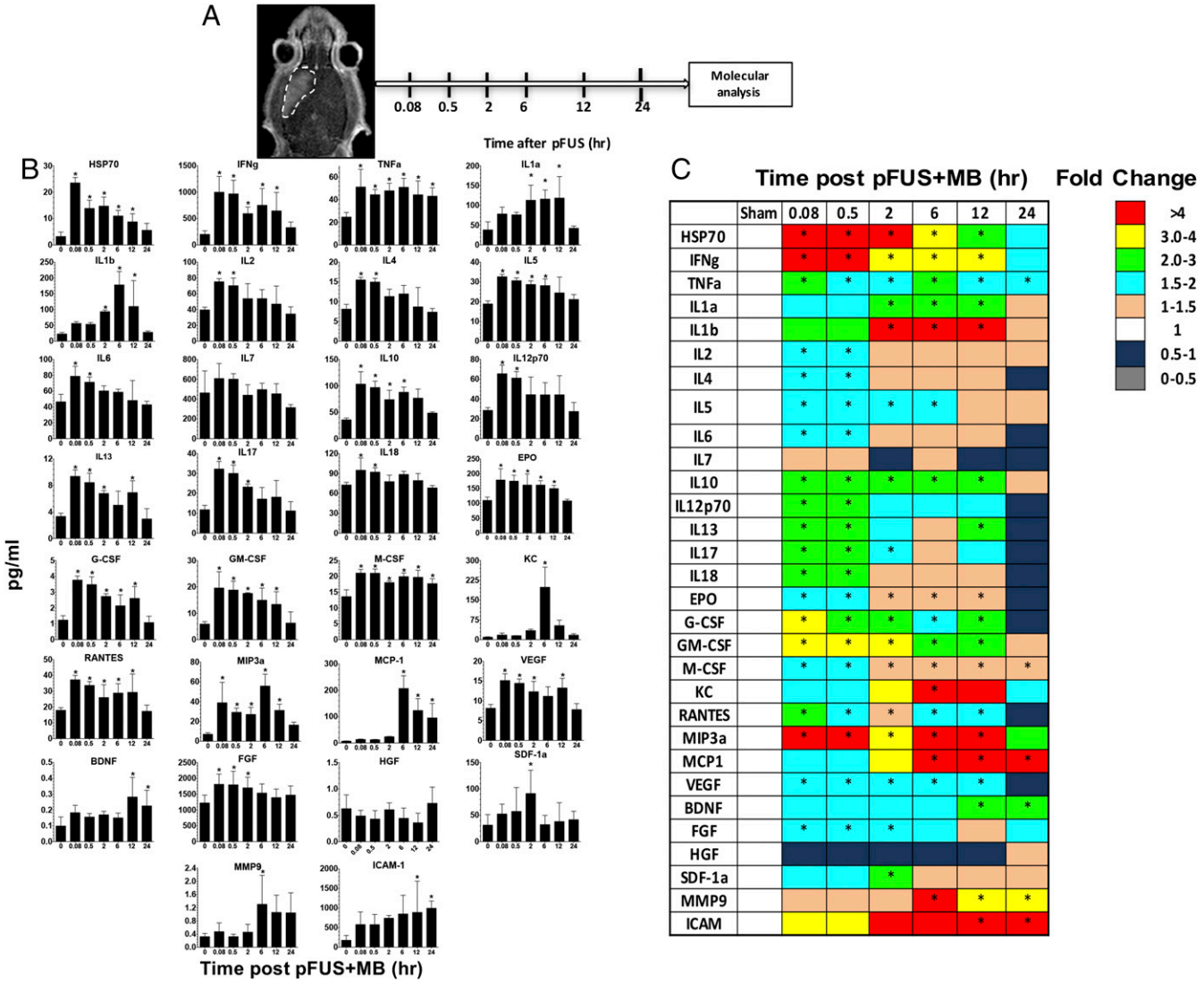

Fig. 2. Molecular changes in the brain following pFUS+MB: pFUS+MB proteomic response in the brain. (*A*) Diagram of the experimental protocol. Post-treatment Gd-enhanced T1w images showing BBBD in rat left cortex and striatum. Brains from treated rats ($n = 5$ per time point) and from sham-treated controls ($n = 5$) were harvested at each time point for molecular analyses. (*B*) Quantification of CCTFs and ICAM in brain after pFUS. The *y* axes represent picograms per milliliter; the *x* axes represent hours post pFUS+MB. For the sham control brains, no pFUS+MB was administered. (*C*) Heat map depicting fold changes in CCTFs and CAM over time after brain exposure to pFUS+MB. Protein levels were quantified by ELISA and were normalized to sham control values. Asterisks indicate statistically significant elevations ($P < 0.05$) identified by ANOVA and Bonferroni post hoc tests.

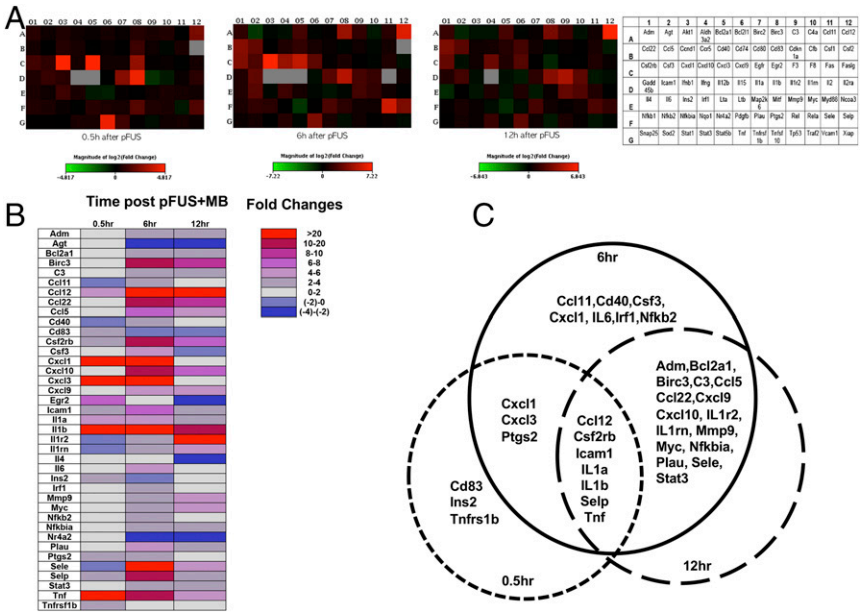

Fig. 3. Changes in mRNA levels after pFUS+MB. (*A*, *Left*) Heat maps derived from qRT-PCR of 84 genes related to the NFκB pathway at 0.5, 6, and 12 h post pFUS+MB at three time points. (*Right*) Key to encoding genes. (*B*) Fold changes were calculated based on the expression level in the contralateral brain. Only fold changes >2 are presented. (*C*) Venn diagrams show the overlap in mRNA expression for each of the three time points. Significant elevations in mRNA expression of Ptgs2 and proinflammatory factors (*Il1a*, *Il1b*, *Ccl12*, and *Tnf*), integrin (*Selp*), and *Icam1* were detected at 30 min after pFUS+MB and lasted for 12 h. At 6 h post pFUS+MB an increase in *Nfkb2* mRNA was detected, supporting proteomic changes that would indicate that pFUS+MB induced a sterile inflammatory response through NFκb pathways. (Significantly elevated genes encoding for mRNA are described in Table S2, and fold changes for the 84 genes evaluated are given in Table S3.)

(Fig. 3 and Table S3). The elevations in mRNA included genes encoding *Nfkb2*, chemotaxis and inflammatory factors (*Ccl11*, *Cd40*, *Csf3*, *Cxcl1*, *Il6*, and *Irf1*), and genes involved in cell survival (*Bcla2a1* and *Birc3*). In addition to the increased mRNA expression of *Mmp9*, urokinase–plasminogen activator (*Plau*) encoding for the degradation of extracellular matrix also was elevated between 6 and 12 h, suggesting a possible effect of sonication on the extracellular proteins. At 12 h postsonication, 24 of 32 mRNAs at 6 h remained elevated by more than twofold compared with the contralateral hemisphere (Fig. 3 and Table S3). Within 6 h postsonication, Western blot analysis revealed significant increases in the expression of the proteins phospho (p)-protein kinase B (Akt) along with phospho (p)-glycogen synthase kinase 3 beta (pGSK3β); these increases are consistent with prosurvival processes (Fig. 4). Other possible signaling pathways, including p38-MAPK, pERK, and pJNK, were not significantly elevated following pFUS+MB to the brain (Fig. S1).

No significant elevations of other DAMPs associated with SIR, such as hypoxia-inducible factor 1 alpha (HIF-1α), high mobility group box 1 protein, receptor for advanced glycation end products (RAGE), or ATP, were observed in sonicated brains (Fig. S2). The inability to detect these DAMPs or to identify alternate inflammatory pathways may result from the time points when samples were collected or possible dilution effects. Taken together, these results indicate that mechanical effects from pFUS+MB–induced sterile inflammation in the brain primarily through NFκB-associated pathways. We did not detect an elevation in caspase 3 (Fig. S2), suggesting that the TUNEL$^+$ cells were damaged neuronal elements.

Histological Alterations Following pFUS+MB. IF histological evaluations of the rat brain following pFUS+MB exposure were performed at 1, 6, and 24 h on three to six adjacent 5–10-μm-thick sections (Figs. 5–7 and Figs. S3 and S4). To investigate if pFUS+MB–induced cellular damage, TUNEL enzymatic staining was performed. With quantitative image analyses, an approximately five- to sevenfold increase ($P < 0.05$, ANOVA) in the number of TUNEL$^+$ cells was observed in the pFUS+MB–targeted cortex compared with contralateral brain between 1 and 6 h postexposure (Fig. 5*A*). There also was a trending increase in TUNEL$^+$ cells at 24 h postsonication compared with contralateral cortex (Fig. 5*A*). Further analysis of TUNEL$^+$ cells at 1 h postsonication revealed that the majority of damaged cells were neurons (NeuN), and a minority were astrocytes (GFAP) (Fig. 5*B*). In response to pFUS+MB, progressively greater expression of ICAM (fourfold compared with contralateral hemisphere; $P < 0.05$) was detected on the endothelium starting at 6 h and peaking at 24 h (Fig. 6 *A* and *D*). The delayed increase in ICAM upon IF staining complements the elevations (more than two- to sixfold) in protein and mRNA expression observed starting as early as 30 min postsonication. Microglial activation [ionized calcium-binding adapter molecule 1 (Iba1)] in the targeted cortex was increased

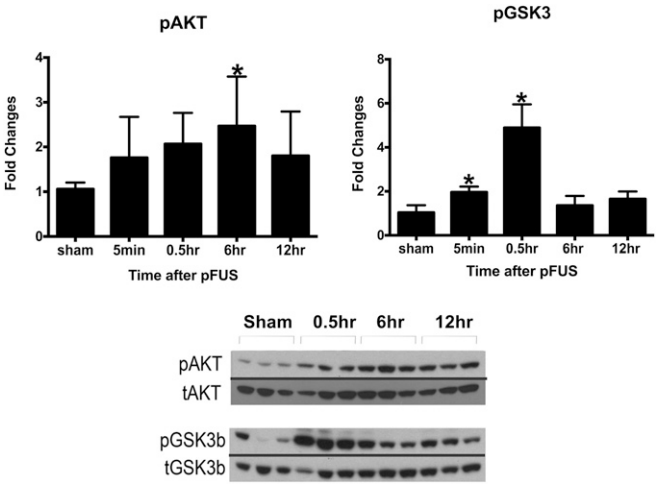

Fig. 4. Changes in the activation of AKT (Ser473) and GSK3β after pFUS+MB. Brain homogenates were prepared in radioimmunoprecipitation assay (RIPA) lysis buffer from brain tissues harvested at 5 min and 0.5, 6, and 12 h after pFUS+MB. Equal amounts of sample proteins (i.e., 25 μg) were loaded, and Western blotting was performed. The activation of protein was quantified as a ratio of phosphorylated to total proteins. The ratio was compared with the sham activation ratio to calculate fold changes in activation. Each time point had $n = 3$ animals, and the data in the graph represent the mean ± SD of at least three independent experiments (one-way ANOVA with multiple comparisons; $*P < 0.05$). The figure was created by splicing the phosphoprotein bands and merging them together with total protein bands for clear and easy representation of changes in phosphoproteins. The blot shown is representative of at least three independent experiments.

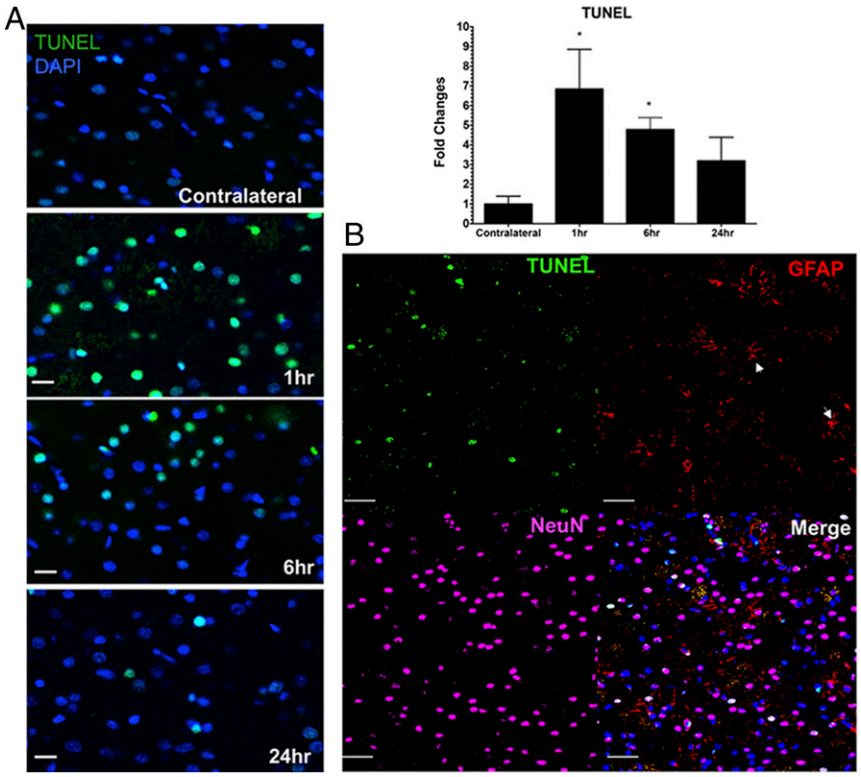

Fig. 5. Evaluation of TUNEL staining following pFUS to the brain. (*A*, *Left*) TUNEL staining revealed a significant sevenfold increase in the number of cells at 1 h and a fivefold increase at 6 h after pFUS+MB that decreased toward the levels in the contralateral cortex by 24 h post pFUS+MB. (*Right*) Quantitative analysis. Quantitation of TUNEL staining was calculated from mean cell counts from 10 FOV per hemisphere in three consecutive sections from each of three rats. Statistical analyses were based on one-way ANOVA with multiple comparisons with the contralateral hemisphere; $*P < 0.05$. Data are presented as mean ± SD. (Scale bars, 100 μm.) (*B*) Confocal micrographs of immunofluorescent TUNEL (green), GFAP (red), NeuN (magenta), DAPI (blue), and merged (white) staining of rat cortex at 1 h post pFUS+MB. Fibrous astrocytes are indicated by white arrowheads. (Scale bars, 100 μm.) (See Fig. S3 for a representative TUNEL-stained whole-brain section.)

significantly (more than twofold; $P < 0.05$, ANOVA) from 1 to 6 h and returned to contralateral levels by 24 h postsonication (Fig. 6 *B* and *D*). Significant elevations ($P < 0.05$, unpaired *t* test) of GFAP were observed, with fibrous astrocyte morphology appearing at 1 h post pFUS+MB and continuing through 24 h (Fig. 6 *C* and *D*). The fibrous appearance would be consistent with astrogliosis associated with inflammatory changes in the parenchyma (Fig. 5*B* and Fig. S5).

To evaluate pFUS+MB effects on the innate immune response, 3 d before sonication rats were infused with fluorescently labeled superparamagnetic iron oxide nanoparticles (FlSPION) to label systemic macrophages in vivo (37). T2*w images obtained 6 d after pFUS+MB revealed more hypointense voxels that are consistent with the migration of FlSPION-labeled cells into the sonicated parenchyma (Fig. 7). IF revealed that the number of $CD68^+$ cells containing intracellular fluorescent beads was about fourfold greater ($P < 0.05$) within the pFUS+MB–treated parenchyma than in the contralateral hemisphere. The increase in chemoattractants following pFUS+MB probably was responsible for the tropism of FLSPION $CD68^+$ macrophages into the parenchyma.

Discussion

The SIR to ischemia, trauma, or noninfectious diseases involves multiple neural and vascular elements that ultimately result in BBBD coinciding with the release of CCTFs and CAM (1, 3–7, 9, 17, 18). Alterations in metabolism and in the structure of cerebral vascular endothelium led to the impairment of the BBB function (i.e., disrupted homeostasis) and to the leakage of blood products into the parenchyma microenvironment (14, 15, 17, 33). pFUS+MB infusions have been used to cause obicodilation (nonthermal FUS to induce MB-mediated BBB opening) to facilitate the delivery of drugs and genes to treat primary and metastatic brain tumors, stroke, or neurodegenerative diseases [i.e., Alzheimer's disease (AD)] (6, 20, 38–40). pFUS exerts acoustic radiation forces on intravascularly confined MB, which undergo stable cavitation. Cavitation forces alter TJP expression and Ca^{2+} flux within the NVU (20, 21, 30, 34, 41). The decrease in or redistribution of TJP results from the transient separation of endothelium observed on EM with immune-gold labeling (41, 42). Moreover, EM of sonicated regions showed increased endothelial cell caveolae and transcytosis of HRP associated with BBBD (41, 42). Another explanation for the BBBD resulting from pFUS+MB exposure is that pFUS+MB increases membrane permeabilization or deformation (30) at the adluminal surfaces of endothelial cells, causing leakage or transcytosis of Gd chelates into the parenchyma and making it possible to visualize the changes noninvasively by MRI (11). Moreover, pFUS+MB has been reported to slow blood perfusion caused by transient vasospasm in 10- to 50-μm-diameter vessels and the leakage of fluorescent dye across the open BBB (31). The changes in vessel reactivity followed by reperfusion could induce hypoxic stress on the endothelium, resulting in BBBD (43). Molecular analysis following pFUS+MB–induced vasospasm (31) has not been investigated adequately, but the increases in protein expression or mRNA reported here in HSP70, TNFα, IL1α, IL1β, VEGF, and EPO would be consistent with decreased perfusion and reperfusion within the targeted parenchyma (9, 12, 19, 44–47). The rapid increase in TNFα and other proinflammatory factors indicates an acute involvement of NVU elements in response to hypoxia or injury (14, 48).

Previous studies have suggested that the mechanism of action by which pFUS+MB exposure results in BBBD was stable acoustic cavitation forces acting at the level of TJP (i.e., vessel centric) stretching apart endothelial cells (6, 20, 28, 30, 41). However, this proposed mechanism does not address how the cavitation forces interact directly with other cells in the NVU. In the current study, the pFUS parameters used were selected to minimize parenchymal damage while still transiently opening the BBB without associated microhemorrhages that have been reported to be an indication of tissue damage (41, 42). Following sonication, brains were harvested at various time points to determine the changes in proteomic and mRNA expression and to elucidate the possible pathways associated with the observed

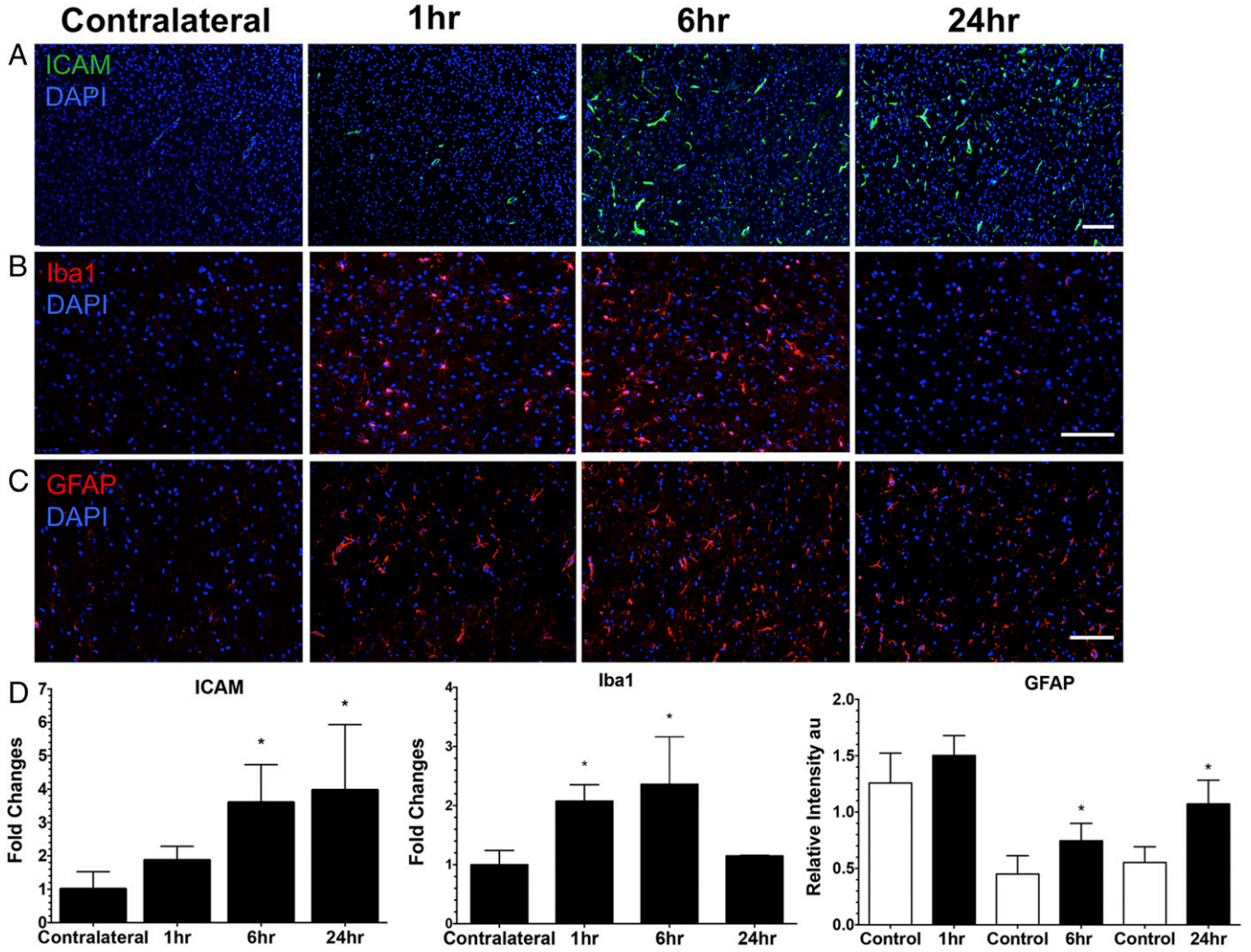

Fig. 6. Histological evaluation of the effect of pFUS+MB in the brain. (*A*) ICAM staining revealed that ICAM expression was significantly elevated beginning at 6 h postsonication, and the elevation persisted through 24 h postsonication. (*B*) Iba1 staining revealed significantly increased Iba1 expression in microglia at 1 and 6 h postsonication in treated brain tissue compared with the contralateral hemisphere. (*C*) GFAP staining revealed activated astrocytes in response to the SIR caused by pFUS+MB. (See Fig. S5 for representative fluorescent GFAP sections of fibrous astrocytes.) GFAP was significantly elevated in the ipsilateral hemisphere at 6 and 24 h compared with the contralateral hemisphere. (*D*) Quantitative analysis for ICAM, GFAP, and Iba1 from sonicated brain at 1, 6, and 24 h. ICAM and Iba1 values were calculated from mean cell counts from 10 FOV per hemisphere in three consecutive sections from each of three rats. For GFAP staining, the area of positive fluorescence signal was calculated using Image J from 10 FOV per hemisphere in three consecutive sections from each of three rats. Statistical analyses were based on one-way ANOVA for multiple comparisons with the contralateral hemisphere (*$P < 0.05$) for ICAM and Iba1 and on a paired *t* test for GFAP ($P < 0.05$). In the GFAP graph the control bars represent the contralateral cortex. Data are presented as mean ± SD. (Scale bars, 100 μm for Iba1 and GFAP; 10 μm for ICAM.) (See Fig. S3 for representative brain sections stained for ICAM, GFAP, and Iba1 and Fig. S4 for isotype control stains.)

BBBD. We propose that because the MBs were confined within vessels in an intact BBB, the effect of pFUS on MB causes cavitation forces that would result in shockwaves (i.e., acoustic pressure waves into the parenchyma) (30) that activate microglia, astrocytes, and neurons beyond the vasculature. BBBD and changes in TJP expression represent one aspect of the effect of pFUS+MB that is associated with triggering the SIR, starting with increases in TNFα and other cytokines (49, 50). Moreover, the increase in VEGF and MCP-1 and Ccl2 gene expression would contribute to BBBD and decrease TJP expression (50). Given the molecular responses that pFUS+MB induced in the brain, cavitation-induced shockwaves may cause cell membrane stretching or damage (51) that ultimately can induce CCTF and CAM expression. The release of CCTFs following pFUS+MB could alter cationic fluxes through stretch-activated channels within the endothelium and neurons (52–54). Stretch-sensitive channels in neurons respond to the shockwaves from pFUS+MB and modulate the influx of cations (e.g., Ca^{+2}) into cells. Low-intensity FUS effects on MB in solution located outside nematodes expressing stretch-sensitive cationic channels resulted in altered behavior and activated neurons following Ca^{+2} influx into cells (55). Low-intensity FUS alone did not induce neuronal activation or alter behavior in the nematodes. These results support our hypothesis that the shockwaves from acoustic cavitation of MB was the primary force behind the increased proteomic and mRNA changes in the sonicated brain. Further studies are needed to determine if radiation forces from pFUS alone at higher peak negative pressures would recapitulate the molecular changes observed when MB were used.

The mechanotransductive (i.e., mechanical stimuli converted into biological activity) effects of pFUS+MB in the brain initiating an SIR accompanied by the release of DAMPs (i.e., HSP70, IL1α) and BBBD are consistent with the activation of NFκB-associated pathways and injury to the NVU (5, 14, 17, 48, 56, 57). Based on

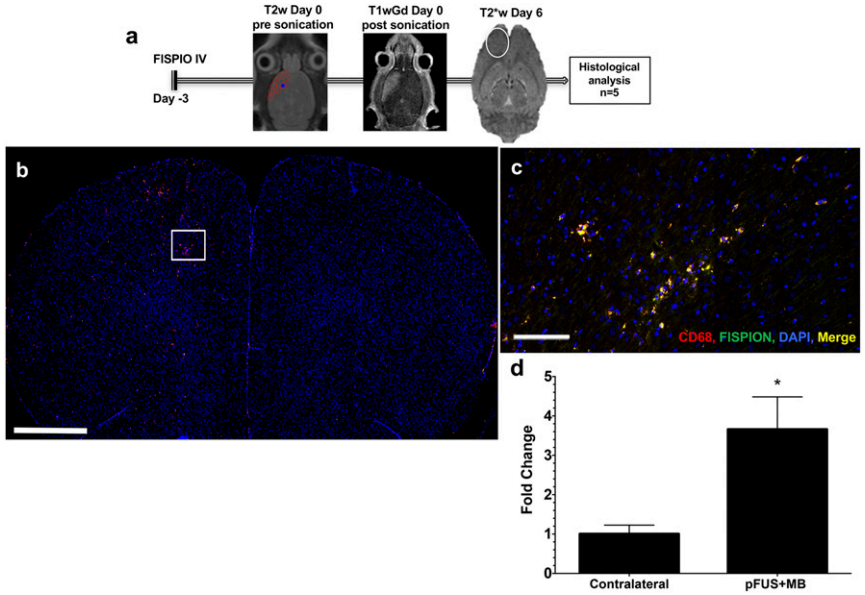

Fig. 7. pFUS+MB induced an innate immune response characterized by the infiltration of CD68$^+$ macrophages. (*A*) A schematic representation of the experimental protocol shows that 3 d before pFUS+MB, rats ($n = 5$) were i.v. injected with FlSPION beads to label macrophages in vivo. pFUS targeting was performed with T2w MRI and postsonication Gd-enhanced T1w MRI to verify opening of the BBB. Six days after pFUS+MB (9 d after FlSPION beads were infused) the area of T2* abnormalities (white oval) in treated cortex was consistent with infiltration of FlSPION-labeled cells into the brain. (*B–D*) Significantly more CD68$^+$-labeled (red) and FLSPION-labeled (green) cells (merged orange) and DAPI-stained nuclei (blue) were observed migrating into the sonicated hemisphere. (*B*) Image of an entire brain section showing more fluorescently labeled CD 68$^+$ cells in the treated hemisphere (left side). The area in the box is the approximate region shown in *C*. (*C*) Magnified epifluorescence microscopy of labeled systemic macrophages in the sonicated hemisphere. (*D*) Fold changes were determined by quantifying the numbers of double-positive (fluorescent for CD68 and FlSPION) cells in each hemisphere over three 10-μm-thick sections and were normalized to the contralateral hemisphere. Data are presented as mean ± SD. Statistical comparisons were made by paired *t* test; $^*P < 0.05$. (Scale bars, 100 μm in *C* and 2 mm in *B*.)

the detected protein and mRNA changes, we hypothesize that the SIR to pFUS+MB was initiated by transient vasospasm and stress reactions in the parenchyma leading to local increases in TNFα, IL1α, IL1β, and IL18 protein or mRNA expression (56, 58). The presence of TNFα and IL1β also would provide a feedback loop to stimulate NFκB pathways and the SIR (58). The increase in IL1β and the presence of albumin in the interstitial spaces has been shown to promote microglial activation (59) and induce the transcription of Ptgs2 (cyclooxygenase 2) detected early after sonications. The prolonged expression of TNFα and IL1β following pFUS+MB has similarities to the temporal proteomic profile obtained by microdialysis from the parenchyma of patients with traumatic brain injuries (60).

The early (i.e., within 2 h post pFUS+MB) increase observed in proinflammatory cytokines presumably originating from activated microglia or macrophages also could be responsible for the delayed protein expression of antiinflammatory cytokines (IL4, IL10, and IL13) and/or neurotrophic factors (BDNF, SDF1α, VEGF, and EPO) as previously reported with BBBD (61–65). The immediate increase in TNFα, IL1α, IL1β, and IL18 could induce the increases in chemotactic factors for immune cells (MCP1, G-CSF, GM-CSF, MIP3α, and RANTES) detected post pFUS+MB (33, 62, 66, 67). Although these chemotactic factors are associated with injury or inflammation, the increased expression of MIP, RANTES, and GM-CSF also may contribute to the closure of the BBB, thereby protecting the brain from further neuronal injury (9, 48, 66, 68). The increased expression of antiinflammatory cytokines (IL4, IL10, and IL13) following pFUS+MB could limit the extent of injury, promote neuronal survival, and induce microglial apoptosis (69–72). Moreover, the increases in EPO (69), SDF1α (7, 73), VEGF (74), BDNF (65, 75), and G-CSF (66) could provide neuroprotection and stimulate neurogenesis and stem cell tropism to sonicated tissue. It is possible that the significantly delayed expression of BDNF protein along with induced antiapoptotic *Bcl2a1* and *Birc3* mRNA would have limited the extent of apoptosis and reactive microglia by 24 h postsonication (65, 75). It has been reported that low-intensity pFUS without MB used in neuromodulation studies increased BDNF expression by CA1 and CA3 neurons in the hippocampus within 45 min, stimulating neurogenesis and brain plasticity (76).

Pulsed FUS+MB has been reported to increase the expression of pAkt along with the downstream signaling molecule pGSK3β at 1.5 h and 24 h, but there are conflicting reports as to whether there are changes in MAPK following sonication of the brain (34, 77). In the current study, transient significant elevations ($P < 0.05$) in pAkt (at 6 h) and pGSK3β (at 5 and 30 min) were detected following pFUS+MB; these elevations declined to baseline levels by 12 h. However, there was no increase in p38-MAPK. The activation of Akt could be the result of oxidative stress observed with cerebral ischemia/hypoxia (78) and/or the expression of proinflammatory cytokines (65) detected following sonication-induced sterile inflammation. The increase in pAkt and pGSK3β might also promote neuronal survival postsonication (77).

Early studies combining pFUS sonications of relatively high peak negative pressures and MB infusions caused microhemorrhages (22, 79, 80); these were avoided by lowering sonication pressures and exposure time (20, 77, 81, 82). Low-intensity pFUS+MB was performed in rabbit brains, and relatively few TUNEL$^+$ cells were detected (42, 80). In the current study, we used pFUS at a peak negative pressure of 0.3 MPa with MB infusions to cause BBBD, and no microhemorrhages were detected (79, 81); however, we observed a significant increase in the number of TUNEL$^+$ cells at 1 and 6 h postsonication. The increase in TUNEL$^+$ cells may be the result of inherent differences in skull thickness and energy absorption or interspecies differences in cerebral physiology.

In vivo prelabeling with FlSPION has been used to track the migration of systemic macrophages by MRI, providing temporal

spatial localization of tagged cells to injured areas following traumatic brain injury (37). We previously reported that in vivo labeling with FlSPION provides the ability after pFUS to track via MRI and histology the homing of these systemic macrophages to pFUS-targeted sites within muscle (83). In our previous study, FlSPION beads were infused 3 d before sonication to provide sufficient time for $CD68^+$ macrophages to endocytose the particles so labeled cells could be tracked by MRI and histology. Moreover, pFUS targeted to tissues also resulted in a shift toward antiinflammatory (M2) rather than proinflammatory (M1) macrophage phenotypes in the absence of histological damage (84, 85). In the current study, 6 d after pFUS+MB, hypointense voxels detected by T2*w MRI and FlSPION-labeled $CD68^+$ macrophages observed via IF staining were scattered throughout the targeted brain. The presence of labeled macrophages is consistent with the local increases in chemotactic factors inducing tropism of immune cells from the circulation to the targeted parenchyma. Further investigation is required to determine the relationship between pFUS+MB treatment and the initial homing of innate immune cells and macrophage phenotypes in the targeted parenchyma.

It has been reported that exposure of the hippocampus to pFUS+MB in AD models revealed microglial phagocytosing beta amyloid precursor protein (βAPP) and increased neurogenesis based on bromo-deoxyuridine uptake or double-cortin staining of proliferating cells (20, 38, 40, 86). Neurobehavioral testing of these treated mice demonstrated improvements in memory function following multiple pFUS+MB exposures. These reports speculated that sonication stimulated neurogenesis, presumably through the release of growth factors, and recommend further studies. Although the molecular mechanisms were not addressed in these AD studies, we have clearly demonstrated that pFUS+MB induces increased expression of CCTFs that could contribute to microglial activation, which in turn could contribute to the clearance of βAPP plaques. Within 2 h after pFUS+MB we detected a significant doubling of IL1β that would activate microglia and clear βAPP plaques from the hippocampus (87). Moreover, the presence of inflammatory cytokines may contribute to the expression of BDNF, EPO, and VEGF in our study and could explain the enhanced neurogenesis observed in AD models (38, 40). Opening of the BBB was associated with the influx of serum products that represent damage signals to microglia, resulting in activation (59). Persistent overexpression of IL1β has been shown to reduce amyloid plaques but to increase phosphorylated tau pathology in an AD mouse model (87). Increased tau has been associated with an increase in GSK3β activity that was observed following pFUS+MB in this study and others (77). Further studies are necessary to investigate the long-term consequences of repeated SIR events following multiple weekly exposures of the brain to pFUS+MB and a role for pFUS+MB as a possible treatment for neurodegenerative diseases.

This study has a few limitations that need to be addressed. The changes in proteomic and transcriptome expression observed following pFUS+MB to the brain were determined only in female rats. It is unknown if the molecular changes we observed are applicable across strains, species, ages, or genders. Because pFUS+MB exerts a mechanical effect and has been shown to cause BBBD in various experimental models, it is likely that the increased expression of CCTFs resulting in a transient SIR would still occur. We also observed a heterogeneous response to pFUS+MB, including variations in contrast enhancement on MRI that was dependent on the distance from the top of the skull and potential energy dissipation of the FUS exposure. The variability in the extent and type of insult to the parenchyma may result from skull thickness or from the sensitivity of the BBB and neuronal elements to the acoustic cavitation forces generated by the pFUS interaction with MB. We also were unable to identify clearly which neuronal cellular elements primarily contributed to the SIR following pFUS+MB. Furthermore, examination of pFUS+MB should be performed in larger animal models mimicking sonication exposures to tumors to determine if SIR is induced within the parenchyma. Further research is needed to determine how the molecular and pathological response to multiple pFUS+MB will impact the reparative or neurodegenerative processes in the targeted brain.

In summary, image-guided pFUS+MB is a clinically relevant, noninvasive technique that can effectively cause transient opening of the BBB and has been used to enhance the retention and permeability of drugs or gene therapy materials within targeted regions in the brain (6, 20, 30, 39). Previous studies have indicated that the mechanical effects of pFUS+MB were confined primarily to the endothelium and vessel wall and were associated with cerebral vasculature vasospasm (31). Within 5 min of pFUS+MB, we observed the transient BBBD and an increased expression of DAMPs leading to an SIR through NFκB pathways that lasted for ∼24 h. Moreover, there was evidence of early neuronal and astrocytic injury, based on TUNEL staining, and astrocyte and microglial activation along with increased expression of CAM. The SIR within the parenchyma influenced the tropism of systemic macrophages to the targeted brain. These results indicate that the mechanotransductive effects of pFUS+MB in the brain require further investigation to determine pFUS+MB's potential clinical contribution to the treatment of neurological diseases.

Methods

Animals. The Animal Care and Use Committee at the National Institutes of Health approved all studies, and experiments were performed according to the National Research Council's Guide for the Care and Use of Laboratory Animals (88). Female 8- to 10-wk-old Sprague–Dawley rats purchased from Charles River Laboratory were used in this study.

MRI-Guided pFUS+MB. Rats were anesthetized with isofluorane [1–3.5% (vol/vol)] and 100% O_2 through a nosecone for all experiments. MRI was performed using a 3-T MR scanner (Achieva Philips Healthcare) using either a surface coil (RK-100; FUS Instruments) or a 3-cm diameter solenoid coil (Philips Research Laboratories). Targeting coordinates were registered (Fig. 1*A*) on axial T2w images of the rat brain acquired before sonication with the following parameters: turbo spin echo (TSE) with repetition time/echo time (TR/TE) = 2,000/70 ms. pFUS was performed with the following parameters: 0.3 MPa acoustic pressure was applied in 10-ms bursts and a 1% duty cycle (120 s per nine focal points) using a single-element spherical FUS transducer (center frequency: 589.636 KHz; focal number: 0.8; active diameter: 7.5 cm) (FUS Instruments). The focal point of the FUS transducer was targeted based on an axial T2w MRI from the anterior cortex to the lateral ventricle with nonoverlapping 2-mm circles (Fig. 1). Sonications were accompanied by MB infusion of 100 μL Optison (GE Healthcare) through the tail vein at a rate of 1 μL/s. After sonication, rats received 200 μL gadofosveset (Ablavar, an albumin-binding chelated Gd formulation; Lantheus Medical Imaging, Inc.) via the tail vein, and axial T1w contrast-enhanced images were obtained with the following parameters: TSE (TR/TE 350/12 ms). High-resolution images following sonication to detect the presence of FlSPION-labeled macrophages were obtained with the following sequences: T2w TSE (TR/TE 2,769/60 ms), T2*w (TR/TE 1,301/7.0 ms), number of echoes 5, ΔTE 7.0 ms, flip angle 30°, T1wGd TSE (TR/TE 600/20 ms).

Molecular Analysis. At 0 (sham, $n = 5$), 0.08, 0.5, 2, 6, 12, and 24 h after sonication, rats ($n = 5$ per time point) were deeply anesthetized with isoflurane before decapitation. The brains were dissected from the skull, and the sonicated tissue and the corresponding sham tissue were isolated. Tissue was snap-frozen in liquid nitrogen and kept at −80 °C until homogenization in cell lysis buffer (9803S; Cell Signaling Technology) containing a protease inhibitor mixture (S8820-2TAB; Sigma-Aldrich). Samples were centrifuged at 15,996 × *g* for 20 min at 4 °C, and the supernatant was used for analyses. Total protein was determined using a bicinchoninic acid (BCA) assay (23227; Thermo Scientific). Homogenates (2 mg/mL total protein) were analyzed by Rat Bio-Plex Cytokine 24-Plex group I assay (171-K1001M; Bio-Rad Laboratories, Inc.) or ELISAs for the following: stromal cell-derived factor 1 (SDF1) (RS0074; NeoBiolab), BDNF (ELR-BDNF; RayBiotech, Inc.), MMP9; FGF (MFB00), ICAM (RIC100), HSP70 (DYC1663-2), and hepatocyte growth factor (HGF) (MHG00), all from R&D Systems, Inc. All assays were performed

according to the manufacturer's protocols. Samples were run with a protein concentration of 2 mg/mL and were read on a spectrophotometric plate reader (Spectra Max M5; Molecular Devices).

RNA Isolation and Quantitative Real-Time PCR. For the assessment sham and NFκB-treated brains were obtained at 0.5, 6, and 12 h after sonication ($n = 3$ per time point) and were extracted into RNAlater (Ambion/Life Technologies) and stored at −20 °C. Between 60 and 70 mg of tissue were homogenized in a Paris Cell Disruption Buffer with Omni Tip probes (Omni International), and RNA was isolated using the Paris RNA Isolation Kit (Ambion/Life Technologies) according to the manufacturer's instructions. cDNA synthesis was performed using the RT^2 First Strand Kit (Qiagen) followed by quantitative RT-PCR (qRT-PCR) using the CFX96 Touch Real-Time PCR Detection System (Bio-Rad Laboratories) with RT^2 SYBR Green qPCR Master Mix (Qiagen). cDNA samples from each time point were screened with RT^2 Profiler PCR Array Rat NFκB Signaling Pathway (Qiagen). Data were analyzed using the SABiosciences PCR Array Data Analysis Web Portal (www.qiagen.com/shop/genes-and-pathways/data-analysis-center-overview-page/).

Western Blotting. Western blotting was performed in samples from sham ($n = 3$) and treated brains obtained at 0.5, 6, and 12 h following sonication ($n = 3$ per time point). Protein (25 μg) was electrophoresed by SDS/PAGE on 4–12% Novex Bis-Tris gels (Invitrogen, Thermo Fisher Scientific) under reducing conditions and was transferred to PVDF membranes. Membranes were blocked in 5% BSA in TBS plus 0.05% Tween-20 (TBST) for 1 h and then were hybridized overnight at 4 °C in TBST containing 2% BSA with rabbit or mouse primary antibodies against following phospho- and total proteins: protein kinase B (Akt), glycogen synthase kinase 3B (GSK3b), ERK, JNK, and p38-MAPK. All antibodies were from Cell Signaling Technology and were used in 1:1,000–1:2,000 dilutions. HIF1α, HMGB-1, and RAGE antibodies were from Thermo Fisher Scientific and were used in 1:1,000 dilutions. Secondary antibodies were HRP-conjugated goat antibodies against mouse or rabbit (Jackson ImmunoResearch Laboratories) used in 1:10,000 dilutions with 1 h incubation at room temperature. Protein bands were detected using the Amersham ECL Prime Western Blotting Detection Reagent (GE Healthcare), and the relative protein amount was measured using ImageJ (National Institutes of Health).

Histological Staining. Rats ($n = 3$ per time point) were killed at 1, 6, and 24 h post pFUS and were perfused with 4% (wt/vol) paraformaldehyde. Fixed brains were embedded in paraffin or optimum cutting temperature (O.C.T.) tissue-mounting medium and were sliced into 5–10-μm sections. Paraffin (p) and frozen (f) tissue sections were stained with H&E and with IF for immunohistochemistry (IHC). Immunostaining of three sections from each animal detected ICAM, GFAP, Iba1, and albumin. Primary antibodies used for IHC were goat anti-ICAM, 1:20 (p) (AF583; R&D Systems Inc.), rabbit anti-GFAP, 1:1,500 (f) (Ab 33922; Abcam), goat anti-Iba1, 1:100 (p) 1:200 (f) (019-19741; Wako Chemicals), and sheep anti-albumin, 1:100 (f) (Ab53435; Abcam). All the secondary antibodies were from Abcam and were used in 1:200 dilutions [goat anti-rabbit antibody (Ab102293; Abcam) for GFAP and Iba1; donkey anti-goat antibody (Ab150129; Abcam) for ICAM; and donkey anti-sheep antibody (Ab150178; Abcam) for albumin]. $TUNEL^+$ cells were detected with an in situ cell-death detection kit (AP 11684809910; Roche Life Science) according to the manufacturer's protocol. Isotype control antibody stains are shown in Fig. S4.

Macrophage Labeling. Three days before pFUS+MB, rats ($n = 5$) were injected via the tail vein with 8 mg/kg MicroTRACK biodegradable rhodamine encapsulated magnetic polymers (CL-01Q02-B-50; BioPal, Inc.). MRI was obtained at 3 T before and 6 d after pFUS+MB exposure. Rats were killed 6 d after sonication. Frozen sections (10 μm thick) were IF-stained for a macrophage marker, CD68, 1:200 (f) (Ab31630; Abcam). Sections were analyzed for colocalized CD68 and nanoparticle-associated rhodamine using Image J and were compared with the contralateral hemisphere.

Microscopy. Microscopy was performed with an Aperio ScanScope CS system equipped with a 20× air objective (NA = 0.75) (Leica Microsystems). High-magnification (60×) images were taken with an Olympus BX61fluorescent microscope. A laser scanning confocal microscope (model 710; Carl Zeiss AG; www.zeiss.com/global/home.html) using Plan-Apochromat objectives (20× air, NA = 0.8) was used for confocal microscopy. Illumination was provided by argon-ion (Lasos, www.lasos.com), diode, and diode-pumped solid-state lasers (Roithner Lasertechnik, www.roithner-laser.com).

Histologic Analysis. Histological evaluation of the microscopy sections was performed at 20× magnification. Fold changes were based on cell counts that were normalized from 10 fields of view (FOV) per hemisphere from three rats using Image J. For GFAP staining, the area of fluorescent signal was quantified using Image J by setting thresholds from 10 FOV per hemisphere of three rats followed by normalization of the pixel area to the contralateral hemisphere.

Statistical Analysis. All values are presented as mean ± SD. Statistical analyses and data presentation were performed with Prism (version 6, GraphPad Software, Inc.). Student's unpaired *t* tests were used for pairwise comparisons, and one-way ANOVA with Bonferroni post hoc tests was used for multiple comparisons. P values < 0.05 were considered significant.

ACKNOWLEDGMENTS. This research was funded by the Intramural Research Programs of the Clinical Center and the National Institute of Biomedical Imaging and Bioengineering at the National Institutes of Health.

1. Schoknecht K, David Y, Heinemann U (2015) The blood-brain barrier-gatekeeper to neuronal homeostasis: Clinical implications in the setting of stroke. *Semin Cell Dev Biol* 38:35–42.
2. Cardoso FL, et al. (2015) Systemic inflammation in early neonatal mice induces transient and lasting neurodegenerative effects. *J Neuroinflammation* 12:82.
3. Daneman R, Prat A (2015) The blood-brain barrier. *Cold Spring Harb Perspect Biol* 7(1):a020412.
4. Cernak I, O'Connor C, Vink R (2002) Inhibition of cyclooxygenase 2 by nimesulide improves cognitive outcome more than motor outcome following diffuse traumatic brain injury in rats. *Exp Brain Res* 147(2):193–199.
5. Denes A, Thornton P, Rothwell NJ, Allan SM (2010) Inflammation and brain injury: Acute cerebral ischaemia, peripheral and central inflammation. *Brain Behav Immun* 24(5):708–723.
6. Leinenga G, Langton C, Nisbet R, Götz J (2016) Ultrasound treatment of neurological diseases–current and emerging applications. *Nat Rev Neurol* 12(3):161–174.
7. Yin W, et al. (2013) The migration of neural progenitor cell mediated by SDF-1 is NF-κB/HIF-1α dependent upon hypoxia. *CNS Neurosci Ther* 19(3):145–153.
8. Shlosberg D, Benifla M, Kaufer D, Friedman A (2010) Blood-brain barrier breakdown as a therapeutic target in traumatic brain injury. *Nat Rev Neurol* 6(7):393–403.
9. Cardoso FL, Brites D, Brito MA (2010) Looking at the blood-brain barrier: Molecular anatomy and possible investigation approaches. *Brain Res Brain Res Rev* 64(2):328–363.
10. Eltzschig HK, Carmeliet P (2011) Hypoxia and inflammation. *N Engl J Med* 364(7):656–665.
11. Hawkins CP, et al. (1990) Duration and selectivity of blood-brain barrier breakdown in chronic relapsing experimental allergic encephalomyelitis studied by gadolinium-DTPA and protein markers. *Brain* 113(Pt 2):365–378.
12. Arvin B, Neville LF, Barone FC, Feuerstein GZ (1996) The role of inflammation and cytokines in brain injury. *Neurosci Biobehav Rev* 20(3):445–452.
13. Famakin BM (2014) The immune response to acute focal cerebral ischemia and associated post-stroke immunodepression: A focused review. *Aging Dis* 5(5):307–326.
14. Gadani SP, Walsh JT, Lukens JR, Kipnis J (2015) Dealing with danger in the CNS: The response of the immune system to injury. *Neuron* 87(1):47–62.
15. Shechter R, Schwartz M (2013) CNS sterile injury: Just another wound healing? *Trends Mol Med* 19(3):135–143.
16. Álvarez S, Muñoz-Fernández MA (2013) TNF-A may mediate inflammasome activation in the absence of bacterial infection in more than one way. *PLoS One* 8(8):e71477.
17. Amantea D, et al. (2015) Rational modulation of the innate immune system for neuroprotection in ischemic stroke. *Front Neurosci* 9:147.
18. Chen GY, Nuñez G (2010) Sterile inflammation: Sensing and reacting to damage. *Nat Rev Immunol* 10(12):826–837.
19. Tuttolomondo A, Pecoraro R, Pinto A (2014) Studies of selective TNF inhibitors in the treatment of brain injury from stroke and trauma: A review of the evidence to date. *Drug Des Devel Ther* 8:2221–2238.
20. Burgess A, Hynynen K (2014) Drug delivery across the blood-brain barrier using focused ultrasound. *Expert Opin Drug Deliv* 11(5):711–721.
21. Hynynen K, McDannold N, Vykhodtseva N, Jolesz FA (2001) Noninvasive MR imaging-guided focal opening of the blood-brain barrier in rabbits. *Radiology* 220(3):640–646.
22. McDannold N, Vykhodtseva N, Hynynen K (2008) Effects of acoustic parameters and ultrasound contrast agent dose on focused-ultrasound induced blood-brain barrier disruption. *Ultrasound Med Biol* 34(6):930–937.
23. Suzuki Y, Nagai N, Umemura K (2016) A review of the mechanisms of blood-brain barrier permeability by tissue-type plasminogen activator treatment for cerebral ischemia. *Front Cell Neurosci* 10:2.
24. Gabathuler R (2010) Approaches to transport therapeutic drugs across the blood-brain barrier to treat brain diseases. *Neurobiol Dis* 37(1):48–57.
25. Kroll RA, Neuwelt EA (1998) Outwitting the blood-brain barrier for therapeutic purposes: Osmotic opening and other means. *Neurosurgery* 42(5):1083–1099, discussion 1099–1100.

26. Neuwelt E, et al. (2008) Strategies to advance translational research into brain barriers. *Lancet Neurol* 7(1):84–96.
27. Stamatovic SM, Keep RF, Andjelkovic AV (2008) Brain endothelial cell-cell junctions: How to "open" the blood brain barrier. *Curr Neuropharmacol* 6(3):179–192.
28. Tung YS, et al. (2010) In vivo transcranial cavitation threshold detection during ultrasound-induced blood-brain barrier opening in mice. *Phys Med Biol* 55(20): 6141–6155.
29. McDannold N, Zhang Y, Vykhodtseva N (2011) Blood-brain barrier disruption and vascular damage induced by ultrasound bursts combined with microbubbles can be influenced by choice of anesthesia protocol. *Ultrasound Med Biol* 37(8):1259–1270.
30. Goertz DE (2015) An overview of the influence of therapeutic ultrasound exposures on the vasculature: High intensity ultrasound and microbubble-mediated bioeffects. *Int J Hyperthermia* 31(2):134–144.
31. Raymond SB, Skoch J, Hynynen K, Bacskai BJ (2007) Multiphoton imaging of ultrasound/Optison mediated cerebrovascular effects in vivo. *J Cereb Blood Flow Metab* 27(2):393–403.
32. Nhan T, et al. (2013) Drug delivery to the brain by focused ultrasound induced blood-brain barrier disruption: Quantitative evaluation of enhanced permeability of cerebral vasculature using two-photon microscopy. *J Control Release* 172(1):274–280.
33. Brough D, Denes A (2015) Interleukin-1α and brain inflammation. *IUBMB Life* 67(5): 323–330.
34. Baseri B, et al. (2012) Activation of signaling pathways following localized delivery of systemically administered neurotrophic factors across the blood-brain barrier using focused ultrasound and microbubbles. *Phys Med Biol* 57(7):N65–N81.
35. Tu TW, et al. (2014) Imaging of spontaneous ventriculomegaly and vascular malformations in Wistar rats: Implications for preclinical research. *J Neuropathol Exp Neurol* 73(12):1152–1165.
36. Stamatovic SM, et al. (2005) Monocyte chemoattractant protein-1 regulation of blood-brain barrier permeability. *J Cereb Blood Flow Metab* 25(5):593–606.
37. Foley LM, et al. (2009) Magnetic resonance imaging assessment of macrophage accumulation in mouse brain after experimental traumatic brain injury. *J Neurotrauma* 26(9):1509–1519.
38. Burgess A, et al. (2014) Alzheimer disease in a mouse model: MR imaging-guided focused ultrasound targeted to the hippocampus opens the blood-brain barrier and improves pathologic abnormalities and behavior. *Radiology* 273(3):736–745.
39. Kovacs Z, et al. (2014) Prolonged survival upon ultrasound-enhanced doxorubicin delivery in two syngenic glioblastoma mouse models. *J Control Release* 187:74–82.
40. Leinenga G, Götz J (2015) Scanning ultrasound removes amyloid-β and restores memory in an Alzheimer's disease mouse model. *Sci Transl Med* 7(278):278ra33.
41. Sheikov N, McDannold N, Sharma S, Hynynen K (2008) Effect of focused ultrasound applied with an ultrasound contrast agent on the tight junctional integrity of the brain microvascular endothelium. *Ultrasound Med Biol* 34(7):1093–1104.
42. Hynynen K, McDannold N, Sheikov NA, Jolesz FA, Vykhodtseva N (2005) Local and reversible blood-brain barrier disruption by noninvasive focused ultrasound at frequencies suitable for trans-skull sonications. *Neuroimage* 24(1):12–20.
43. Eltzschig HK, Eckle T (2011) Ischemia and reperfusion–from mechanism to translation. *Nat Med* 17(11):1391–1401.
44. Huang T, et al. (2014) Hypoxia-inducible factor-1α upregulation in microglia following hypoxia protects against ischemia-induced cerebral infarction. *Neuroreport* 25(14): 1122–1128.
45. Lin Y, Wen L (2013) Inflammatory response following diffuse axonal injury. *Int J Med Sci* 10(5):515–521.
46. Lu KT, Wang YW, Wo YY, Yang YL (2005) Extracellular signal-regulated kinase-mediated IL-1-induced cortical neuron damage during traumatic brain injury. *Neurosci Lett* 386(1):40–45.
47. Taupin V, Toulmond S, Serrano A, Benavides J, Zavala F (1993) Increase in IL-6, IL-1 and TNF levels in rat brain following traumatic lesion. Influence of pre- and post-traumatic treatment with Ro5 4864, a peripheral-type (p site) benzodiazepine ligand. *J Neuroimmunol* 42(2):177–185.
48. Amantea D, et al. (2014) Understanding the multifaceted role of inflammatory mediators in ischemic stroke. *Curr Med Chem* 21(18):2098–2117.
49. Capaldo CT, Nusrat A (2009) Cytokine regulation of tight junctions. *Biochim Biophys Acta* 1788(4):864–871.
50. Yao Y, Tsirka SE (2014) Monocyte chemoattractant protein-1 and the blood-brain barrier. *Cell Mol Life Sci* 71(4):683–697.
51. Krasovitski B, Frenkel V, Shoham S, Kimmel E (2011) Intramembrane cavitation as a unifying mechanism for ultrasound-induced bioeffects. *Proc Natl Acad Sci USA* 108(8): 3258–3263.
52. Spangenburg EE, McBride TA (2006) Inhibition of stretch-activated channels during eccentric muscle contraction attenuates p70S6K activation. *J Appl Physiol (1985)* 100(1):129–135.
53. Coste B, et al. (2012) Piezo proteins are pore-forming subunits of mechanically activated channels. *Nature* 483(7388):176–181.
54. Li J, et al. (2014) Piezo1 integration of vascular architecture with physiological force. *Nature* 515(7526):279–282.
55. Ibsen S, Tong A, Schutt C, Esener S, Chalasani SH (2015) Sonogenetics is a non-invasive approach to activating neurons in Caenorhabditis elegans. *Nat Commun* 6:8264.
56. Mohamed IN, Ishrat T, Fagan SC, El-Remessy AB (2015) Role of inflammasome activation in the pathophysiology of vascular diseases of the neurovascular unit. *Antioxid Redox Signal* 22(13):1188–1206.
57. Savage CD, Lopez-Castejon G, Denes A, Brough D (2012) NLRP3-inflammasome activating DAMPs stimulate an inflammatory response in glia in the absence of priming which contributes to brain inflammation after injury. *Front Immunol* 3:288.
58. Singhal G, Jaehne EJ, Corrigan F, Toben C, Baune BT (2014) Inflammasomes in neuroinflammation and changes in brain function: A focused review. *Front Neurosci* 8:315.
59. Ransohoff RM, Perry VH (2009) Microglial physiology: Unique stimuli, specialized responses. *Annu Rev Immunol* 27:119–145.
60. Helmy A, Carpenter KL, Menon DK, Pickard JD, Hutchinson PJ (2011) The cytokine response to human traumatic brain injury: Temporal profiles and evidence for cerebral parenchymal production. *J Cereb Blood Flow Metab* 31(2):658–670.
61. Burda JE, Bernstein AM, Sofroniew MV (2016) Astrocyte roles in traumatic brain injury. *Exp Neurol* 275(Pt 3):305–315.
62. Hedtjärn M, et al. (2002) Interleukin-18 involvement in hypoxic-ischemic brain injury. *J Neurosci* 22(14):5910–5919.
63. Sofroniew MV (2015) Astrocyte barriers to neurotoxic inflammation. *Nat Rev Neurosci* 16(5):249–263.
64. Takamiya M, Fujita S, Saigusa K, Aoki Y (2007) Simultaneous detections of 27 cytokines during cerebral wound healing by multiplexed bead-based immunoassay for wound age estimation. *J Neurotrauma* 24(12):1833–1844.
65. Zhou J, Ping FF, Lv WT, Feng JY, Shang J (2014) Interleukin-18 directly protects cortical neurons by activating PI3K/AKT/NF-κB/CREB pathways. *Cytokine* 69(1):29–38.
66. Kelso ML, Elliott BR, Haverland NA, Mosley RL, Gendelman HE (2015) Granulocyte-macrophage colony stimulating factor exerts protective and immunomodulatory effects in cortical trauma. *J Neuroimmunol* 278:162–173.
67. Thompson WL, Van Eldik LJ (2009) Inflammatory cytokines stimulate the chemokines CCL2/MCP-1 and CCL7/MCP-3 through NFkB and MAPK dependent pathways in rat astrocytes [corrected]. *Brain Res* 1287:47–57.
68. Tokami H, et al.; REBIOS Investigators (2013) RANTES has a potential to play a neuroprotective role in an autocrine/paracrine manner after ischemic stroke. *Brain Res* 1517:122–132.
69. Marti HH (2004) Erythropoietin and the hypoxic brain. *J Exp Biol* 207(Pt 18): 3233–3242.
70. Shin WH, et al. (2004) Microglia expressing interleukin-13 undergo cell death and contribute to neuronal survival in vivo. *Glia* 46(2):142–152.
71. Strle K, et al. (2001) Interleukin-10 in the brain. *Crit Rev Immunol* 21(5):427–449.
72. Yang MS, et al. (2006) Interleukin-13 enhances cyclooxygenase-2 expression in activated rat brain microglia: Implications for death of activated microglia. *J Immunol* 177(2):1323–1329.
73. Stumm RK, et al. (2002) A dual role for the SDF-1/CXCR4 chemokine receptor system in adult brain: Isoform-selective regulation of SDF-1 expression modulates CXCR4-dependent neuronal plasticity and cerebral leukocyte recruitment after focal ischemia. *J Neurosci* 22(14):5865–5878.
74. Kilic E, et al. (2006) The phosphatidylinositol-3 kinase/Akt pathway mediates VEGF's neuroprotective activity and induces blood brain barrier permeability after focal cerebral ischemia. *FASEB J* 20(8):1185–1187.
75. Wang H, Ward N, Boswell M, Katz DM (2006) Secretion of brain-derived neurotrophic factor from brain microvascular endothelial cells. *Eur J Neurosci* 23(6):1665–1670.
76. Tufail Y, et al. (2010) Transcranial pulsed ultrasound stimulates intact brain circuits. *Neuron* 66(5):681–694.
77. Jalali S, Huang Y, Dumont DJ, Hynynen K (2010) Focused ultrasound-mediated bbb disruption is associated with an increase in activation of AKT: Experimental study in rats. *BMC Neurol* 10:114.
78. Song YS, et al. (2008) The role of Akt signaling in oxidative stress mediates NF-kappaB activation in mild transient focal cerebral ischemia. *J Cereb Blood Flow Metab* 28(12): 1917–1926.
79. Hynynen K, McDannold N, Martin H, Jolesz FA, Vykhodtseva N (2003) The threshold for brain damage in rabbits induced by bursts of ultrasound in the presence of an ultrasound contrast agent (Optison). *Ultrasound Med Biol* 29(3):473–481.
80. McDannold N, Vykhodtseva N, Raymond S, Jolesz FA, Hynynen K (2005) MRI-guided targeted blood-brain barrier disruption with focused ultrasound: Histological findings in rabbits. *Ultrasound Med Biol* 31(11):1527–1537.
81. Konofagou EE (2012) Optimization of the ultrasound-induced blood-brain barrier opening. *Theranostics* 2(12):1223–1237.
82. McDannold N, Arvanitis CD, Vykhodtseva N, Livingstone MS (2012) Temporary disruption of the blood-brain barrier by use of ultrasound and microbubbles: Safety and efficacy evaluation in rhesus macaques. *Cancer Res* 72(14):3652–3663.
83. Burks SR, et al. (2011) Investigation of cellular and molecular responses to pulsed focused ultrasound in a mouse model. *PLoS One* 6(9):e24730.
84. Burks SR, et al. (2015) Pulsed focused ultrasound pretreatment improves mesenchymal stromal cell efficacy in preventing and rescuing established acute kidney injury in mice. *Stem Cells* 33(4):1241–1253.
85. Burks SR, Ziadloo A, Kim SJ, Nguyen BA, Frank JA (2013) Noninvasive pulsed focused ultrasound allows spatiotemporal control of targeted homing for multiple stem cell types in murine skeletal muscle and the magnitude of cell homing can be increased through repeated applications. *Stem Cells* 31(11):2551–2560.
86. Scarcelli T, et al. (2014) Stimulation of hippocampal neurogenesis by transcranial focused ultrasound and microbubbles in adult mice. *Brain Stimulat* 7(2):304–307.
87. Ghosh S, et al. (2013) Sustained interleukin-1β overexpression exacerbates tau pathology despite reduced amyloid burden in an Alzheimer's mouse model. *J Neurosci* 33(11):5053–5064.
88. National Research Council (2011) *Guide for the Care and Use of Laboratory Animals* (National Academy Press, Washington, DC), 1st Ed.